Int. J. Electrochem. Sci., 14 **(2019)** 9711 – 9725, doi: 10.20964/2019.10.24

International Journal of
ELECTROCHEMICAL
SCIENCE
www.electrochemsci.org

Effect of AC Interference on Corrosion Behavior of X100 Pipeline Steel with Different Microstructure in Alkaline Soil Environment

Min Zhu[*], *Jun Ma, Yongfeng Yuan, Shaoyi Guo*

School of Mechanical Engineering & Automation, Zhejiang Sci-Tech University, Hangzhou 310018, PR China
[*]E-mail: zmii666@126.com

Received: 24 May 2019 / *Accepted:* 31 July 2019 / *Published:* 30 August 2019

Alternating current (AC) corrosion behavior of X100 pipeline steel with welded joint in simulated solution of Golmud alkaline soil was studied by electrochemical tests, immersion test and surface analysis technique. Without the presence of AC or at the low AC current densities of 30A·m^{-2} and 50A·m^{-2}, oxygen consumption reaction controls the entire cathode process. While cathode process is dominated by hydrogen evolution reaction at high AC current density of 150A·m^{-2}. With or without AC application, X100 steels with different microstructure have various corrosion resistances, and the corrosion resistance of steels is in the order of normalized > hot rolled > annealed. The pearlite and granular bainite in the steel have high electrochemical activity, where pitting corrosion generally easy to occur. The combined action of temperature and AC current density promotes the corrosion of X100 pipeline steel to a certain extent. At the low AC current density, the effect of temperature on corrosion behavior is more notable. While the AC current density increases up to 150A·m^{-2}, the AC corrosion plays a dominant role.

Keywords: X100 steel; Microstructure; AC interference; Corrosion behavior

1. INTRODUCTION

Due to the increasing development of high-voltage power transmission, rail transit systems and their sharing common right-of-way with the pipes, AC induced corrosion is becoming the significant threat to pipeline transportation [1].Different models and theories have been proposed about the mechanism of AC corrosion. Studies [2-3] have shown that AC currents density induced by buried pipelines can accelerate the corrosion. Kuang et al. [4] have presented that in high pH and near-neutral solutions, AC interference can induce pitting corrosion on the steel surface. Wan et al. [5] found that the negative half-wave AC reduced the corrosion potential, increased the corrosion current density and

generated the local anodic dissolution, such as nuclear pits. This phenomenon indicated that the application of AC accelerated the corrosion of X80 pipeline steel. Xu and Cheng [6] showed that imposed AC promoted ion migration, improved ion activity, and increased the chances of ionic reaction. Zhu Min et al. [7-9] studied the AC current density and frequencies effects on the SCC behavior and mechanism of X80 steel in high pH solution and found that applying AC current density obviously enhanced the SCC susceptibility of the steel. Thus, AC corrosion research is mainly aimed at X80 steel and the low-grade steel, the AC corrosion research on high-grade steel such as X100 steel is very limited.

X100 as a low carbon alloy steel pipeline steel has high mechanical properties and welding performance. It also has great application potential in long-distance pipeline construction. Although there have been increasing literatures of corrosion behavior about X100 in the past [10-11], the subject about AC-induced corrosion of X100 is rare. Thus, the study of AC interference on the corrosion behavior of X100 pipeline steel is necessary to be carried out.

The long distance oil and gas transportation pipelines have a large number of welded joints. The microstructure of the welded joint area is complex and unstable. So these parts are highly prone to corrosion failure [12-14]. In addition, some oil and gas pipelines need to pass through the saline alkaline soil areas, which is one of the soil environments lead to corrosion failure of pipeline steel. West–East natural gas transmission project made use of pipeline steel which runs more than 4000 km across salty soil area (some area called as Golmud soil) in China. The soil solution mainly contains alkalinity and salt content [15-16].Based on the above analysis, AC interference may induce and accelerate the corrosion of pipeline steel in the alkaline soil environment, especially the welded joints. But there is no relevant report on the correlation of microstructure of the welded joints of X100 pipeline steel, AC corrosion behavior, and the influence of temperature. Therefore, the AC corrosion behavior of X100 steel with different microstructure in Golmud soil simulated solution is studied in the paper by electrochemical test and immersion experiment, which provided relevant reference for corrosion protection of X100 steel welded joint.

2. EXPERIMENTAL

The experimental material was a hot-rolled sheet of X100 pipeline steel, and the composition of the steel is as follow(wt %): C 0.04, Si 0.20, Mn 1.55, Mo 0.02, Al 0.02, Cu 0.25, Ni 0.13, Ti 0.02, Nb 0.052,Cr 0.016 and Fe balance. In order to simulate the welded joint of X100 steel, the hot rolled microstructure of X100 steel is treated with different kinds of heat treatment methods. The heat treatment processes were as follows: heating the same size (10mm×10mm×3mm) of X100 steel specimens with hot rolled microstructure to 1150°C in a box-type resistance furnace, keeping for 30 min, and then air cooling the sample to room temperature for normalized microstructure and cooling the other samples to room temperature in the furnace for annealed microstructure. The X100 steel with hot-rolled microstructure, annealed microstructure and normalized microstructure were respectively as working electrodes. Before the experiment, the working surface of the electrodes were ground sequentially from 320# to 2000# of waterproof abrasive paper, followed by rinsing with deionized

water and ethanol, and finally dried in the air. The soil environment of Golmud is a simulation study medium. According to the main physical and chemical data of Golmud soil, the simulated solution components are: 11.34% Cl^-, 0.262% SO_4^{2-}, 0.0099% HCO_3^-, pH 9. The experimental solutions were all equilibrated with analytically pure NaCl, Na_2SO_4, $NaHCO_3$ and deionized water.

The Princeton 2273 PARSTAT electrochemical workstation is used for a conventional three-electrode system, where the counter electrode is a sheet of Pt and a saturated calomel electrode (SCE) served as the reference electrode. DS345 integrated function signal generator is performed for the AC interference. The temperature of the medium is stabilized by using a digital constant temperature water bath. The sample was polarized at a potential of -1000 mV for 3 min before the test to remove the oxide film formed in the air. Then the sample was placed in simulated solution of Golmud alkaline soil for 30 min before the test, and the open circuit potential was stabilized for 1800s. For electrochemical impedance spectroscopy (EIS), the frequency range was 10^5~10^{-2} Hz and the excitation signal amplitude was 10mV. When measuring the polarization curve, the potential sweep range is -300 (vs SCE) ~ -1000 mV (vs SCE), the scan rate is 1 mV/s.

When the potentiodynamic polarization curve is measured under AC interference, measurement parameter is the same as described above. In order to apply the alternating current, there is a sine wave signal with a frequency of 50 Hz is applied during the test. The AC current densities were 30, 50, and 150 $A \cdot m^{-2}$, respectively. The test device diagram was consistent with our previous experimental studies [7-9].

Before the immersion test, the prepared sample was weighed on an electronic balance with an accuracy of one thousandth, and the weight of the sample before test was recorded. The experimental samples were then immersed in alkaline soil simulation solution for a period of 336 h. During the experiment, the applied AC current density (50 Hz) is $100A \cdot m^{-2}$ and the solution temperature is maintained at 35℃. After the immersion test, the weight of each sample after removing the corrosion products was recorded, and then the corrosion rate was calculated. Scanning electron microscopy is used to observe the microscopic corrosion morphology after removing corrosion products.

3. RESULTS

3.1. Metallographic analysis

Fig.1 shows the microstructure of different X100 steels. Fig.1 (a) and (b) exhibit that the hot rolled X100 steel contains a large number of fine and irregular acicular ferrite (AF), and the grain boundaries are blurred. There is no complete continuous grain boundary. A small amount of large polygonal ferrite (PF) can be clearly observed, and more granular bainite (GB) and bright white M/A islands are staggered at the ferrite grain boundaries. The annealed X100 steel in Fig.1(c) and (d) contains lots of quasi-polygonal ferrite (QPF). The microstructures are regular-shaped polygons with some pearlite (P) and GB. As seen in Fig.1 (e) and (f), the size of AF in normalized microstructure is larger than that within hot rolled microstructure. Due to the rapid cooling rate during heat treatment, the M/A in the normalized microstructure does not show the shape of island yet needle-like. Thus the

number of small needle-shaped M/A islands in the microstructure increases significantly.

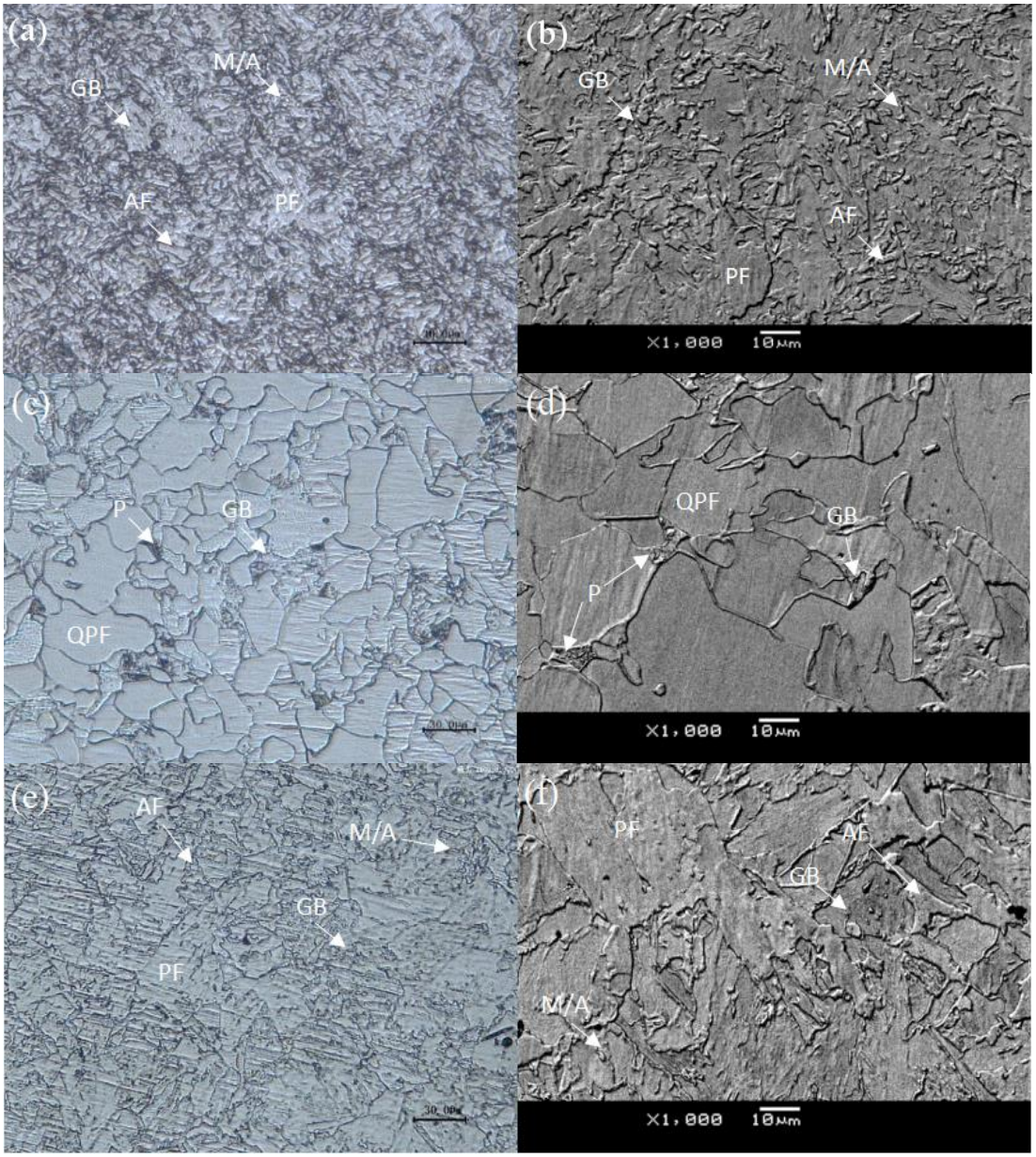

Figure 1. Microstructure of X100 steels with different microscopic structure:**(a,b)** hot-rolled; **(c,d)** annealed; **(e,f)**Normalized.

3.2. Electrochemical test without AC application

The open circuit potential (OCP) of X100 steel with different microstructure as a function of time is displayed in Fig. 2. The OCP of normalized microstructure is more positive than the other two microstructure steels, which of the annealed microstructure is the most negative and the OCP of hot rolled microstructure is between the above two. Generally, the level of the OCP can reflect the corrosion tendency of metal material in the electrolyte solution. The higher the potential, the harder the corrosion occurs. And the lower the potential, the more likely the corrosion will occur. It can be seen

that the annealed microstructure has the highest corrosion tendency and the normalized structure has the least corrosion tendency.

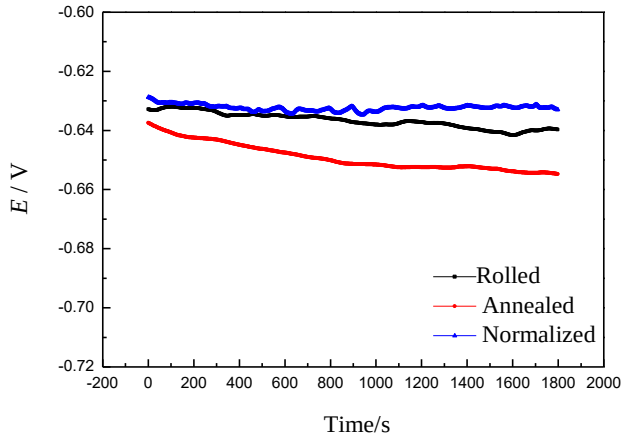

Figure 2. Open circuit potential (OCP) of X100 steels with different microstructure in alkaline soil simulation solution

EIS test was adopted to further investigate the corrosion resistance of X100 steels with different microstructure. The results of EIS test are presented in Fig.3. Fig.3 (a) depicts that the Nyquist plots of X100 steels with different microstructure. The shape of Nyquist curves is similar, which suggests a double capacitive loop. The capacitive radius of the normalized microstructure steel is the largest, that of the annealed microstructure is the smallest and which of the hot rolled microstructure is also between them. As seen in Fig. 3(b), the impedance value of normalized microstructure in the low frequency region is larger than that of the other two microstructures. Fig. 3(c) shows two apparent phase angle peaks, which indicates that two time constants appear when the electrode reaction occurs.

The equivalent circuit $R_s(Q_f(R_f(C_{dl}R_{ct})))$ is used to fit the experiments data of EIS, which is listed in Fig.4. In the circuit, where R_s is solution resistance, R_f is resistance of corrosion product film, Q_f is corrosion product film capacitance, C_{dl} is double-layer capacitance and R_{ct} is charge transfer resistance. The corrosion rate is inversely proportional to the R_{ct}, and a large value R_{ct} means a lower corrosion rate [17–19]. That is, the corrosion rate of materials is mainly affected by the charge transfer rate [20]. The fitted R_{ct} is shown in Fig. 5. As shown in Fig. 5, R_{ct} is in the order of normalized > hot rolled > annealed, thereby the corrosion reaction rate is normalized < hot rolled < annealed.

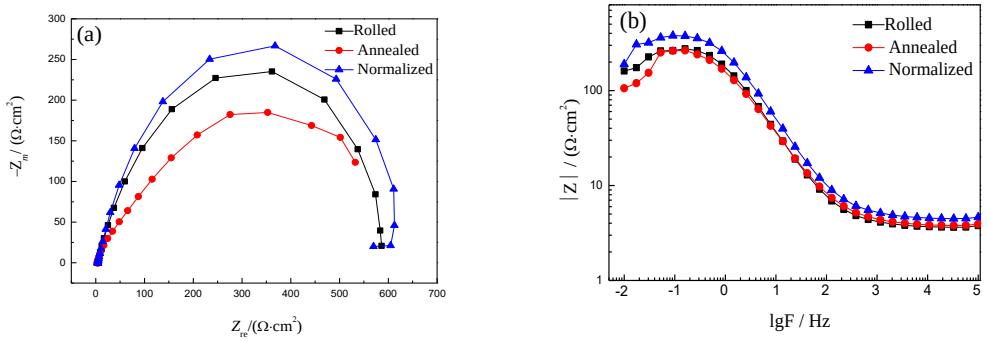

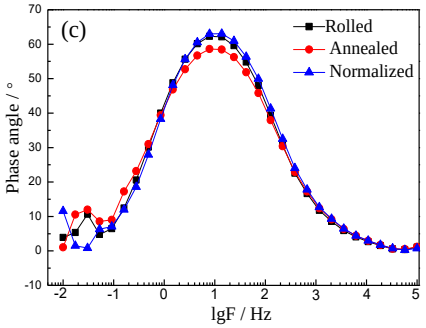

Figure 3. Electrochemical impedance spectra of X100 steels with different microstructure in alkaline soil simulation solution: (a) Nyquist; (b,c) Bode plots.

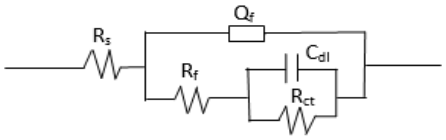

Figure 4. Equivalent circuit diagram of impedance diagram

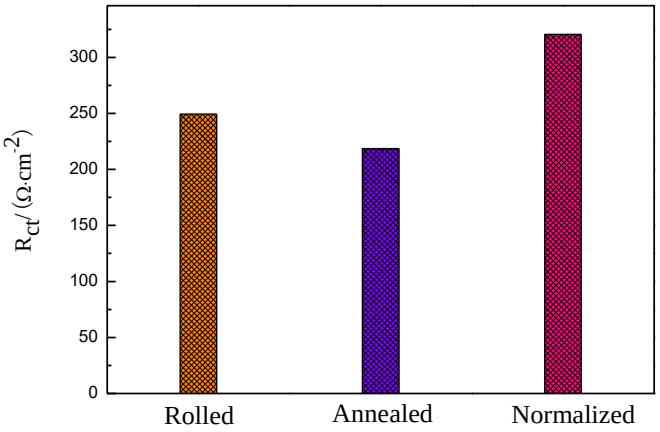

Figure 5. Charge transfer resistance of X100 steels with different microstructure in alkaline soil simulation solution

Fig.6 shows potentiodynamic polarization curves and corrosion current density (I_{corr}) of X100 steels with different microstructure. It is obvious that the anode curves of the polarization curves exhibit activated dissolution characteristics. The cathode of the polarization curve mainly exhibits the characteristic of oxygen-consuming corrosion. Corrosion current density (I_{corr}) is proportional to corrosion rate [20]. The I_{corr} of the annealed structure X100 steel is greater than the other two structures. Therefore, the corrosion rate of the annealed structure (V_a) is the maximum. And the second is the corrosion rate of hot rolled structure (V_h).The normalized structure has the smallest corrosion rate (V_n). Thus, the corrosion rate in the order of $V_a > V_h > V_n$.

Based on the results of the above three electrochemical tests, X100 pipeline steels with different microstructure have various corrosion resistance. Without AC application, the corrosion resistance of X100 steel is in the order of normalized > hot rolled > annealed.

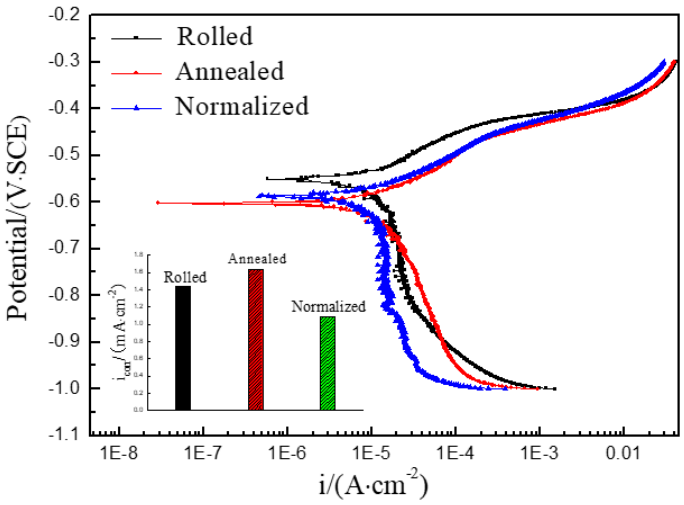

Figure 6. Potentiodynamic polarization curves and corrosion current densities (i_{corr}) of X100 steels with different microstructure tested without AC application in alkaline soil simulation solution

3.3 Polarization curves under different AC current densities

The potentiodynamic polarization curves of X100 steels with different microstructure under various AC current densities are shown in Fig. 7. It can be seen that the corrosion potential undergoes a certain degree of negative shift with the increase of AC current density. Especially at the higher AC current densities, the negative shift of corrosion potential is more obvious. The anode curves exhibit activated dissolution characteristics. When applying the low AC current densities (30 $A \cdot m^{-2}$ and 50 $A \cdot m^{-2}$), the cathode of the polarization curve mainly exhibits the characteristic of oxygen-consuming corrosion. However, as the AC current density increases, the hydrogen evolution reaction gradually appears and ultimately dominates the entire cathodic reaction. Fig.8 clearly shows that as the applied AC density increases, the overall trend of the fitted corrosion current density rises, indicating that AC interference promotes the occurrence of corrosion, especially at higher AC current density.

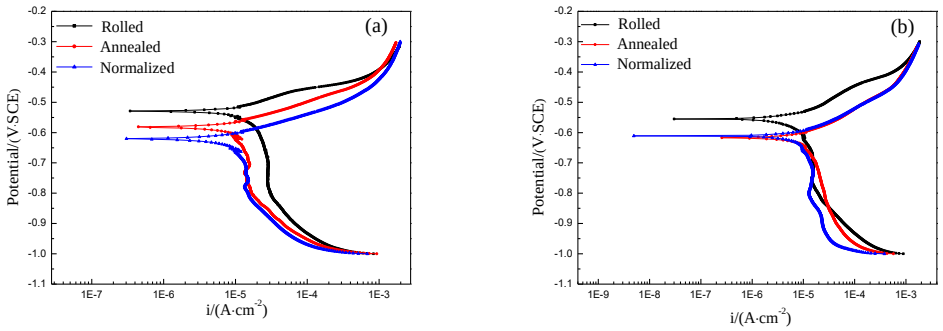

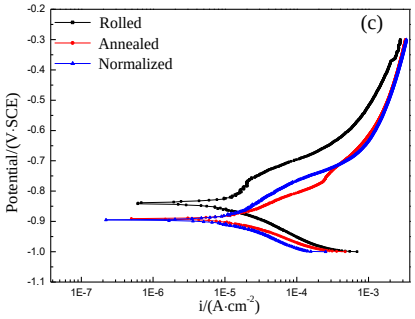

Figure 7. Potentiodynamic polarization curves of X100 steels with different microstructure under various AC current densities in alkaline soil simulation solution: **(a)** 30A·m^{-2}; **(b)** 50A·m^{-2}; **(c)** 150A·m^{-2}

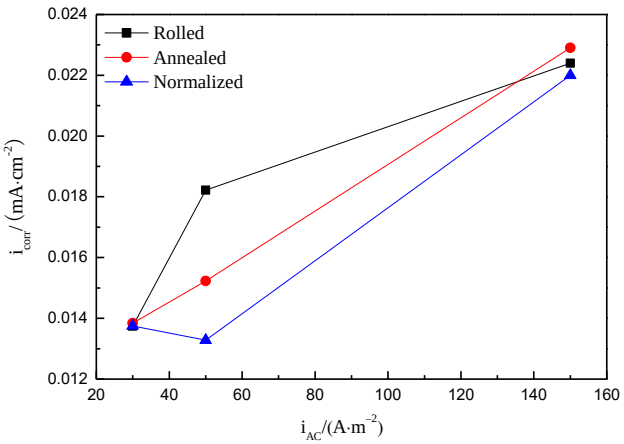

Figure 8. Corrosion current density of X100 steels with different microstructure under various AC current densities in alkaline soil simulation solution

Fig.9 shows the potentiostatic polarization curves of X100 steels with different microstructure under various AC current densities. As seen from Fig.9, the potentiostatic polarization test is divided into three stages:

(1) From 0 to 300s, there is no the application of imposed AC, the corrosion current density of X100 steels with different microstructure increases slowly, which means that the corrosion rate of steels at the constant corrosion potentials are very slow.

(2) From 300 to 900s, the application of AC interference is in the stage. It can be seen that as the applied AC density increases, the corrosion current density of the three kinds of steels exhibits a sharp increase. Compared with the normalized microstructure samples, the hot-rolled and annealed microstructure specimens have a larger increasing trend.

(3) From 900 to 1200s, when the applying of AC interference is removed, the corrosion current density of the X100 steels with different microstructure decreases, but which cannot be restored to the original position.

Thus, under the AC interference, the normalized microstructure steel has the best corrosion resistance under AC application, followed by the hot-rolled microstructure, and the annealed steel exhibits the worst corrosion resistance. The test results are in accord with that of potentiodynamic

polarization curve.

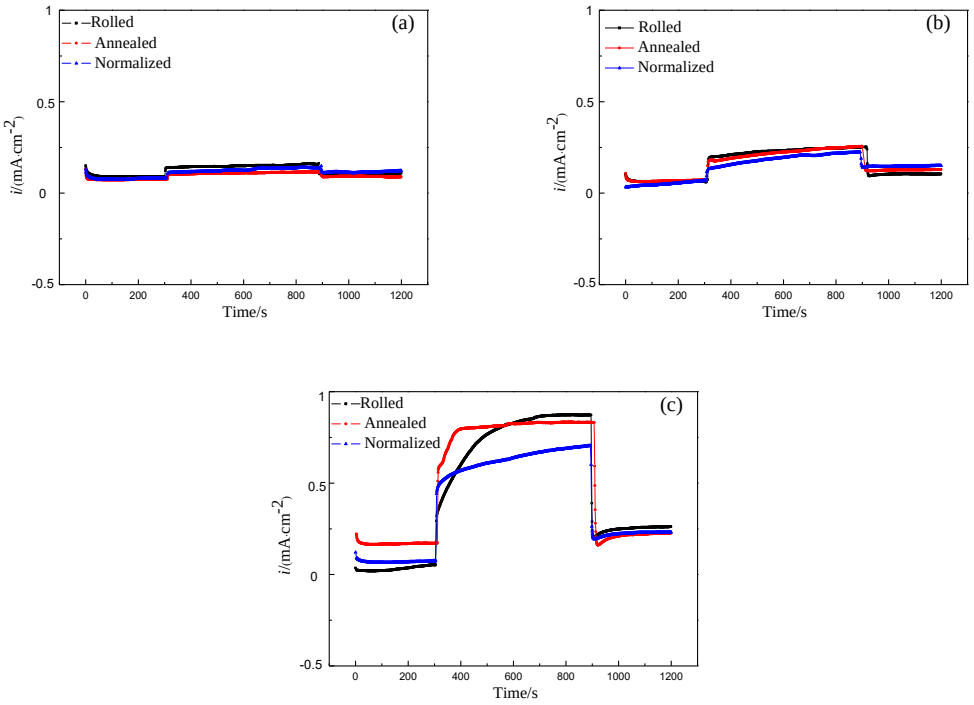

Figure 9. Potentiostatic polarization curves of X100 steels with different microstructure under various AC current densities in alkaline soil simulation solution: **(a)** 30A·m^{-2}; **(b)** 50A·m^{-2}; **(c)** 150A·m^{-2}

3.4. Immersion test

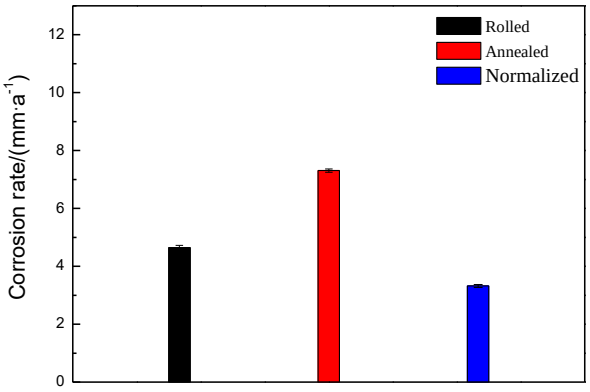

Figure 10. Corrosion rates of X100 steels with different microstructure under AC interference of 100 A·m^{-2} in alkaline soil simulation solution.

The corrosion rates of X100 steels with different microstructure under the same AC interference conditions are revealed in Fig. 10. Obviously, the corrosion rate of X100 steel after

annealing is the largest, which is 7.307mm/a. While the normalized steel has the lowest corrosion rate, which is 3.321mm/a. Different microstructure X100 steels show the various corrosion rates. This indicates under AC interference, the corrosion rate of X100 steel is related to different microstructure.

The surface corrosion morphologies after removing corrosion products of X100 steels with different microstructure are shown in Fig.11.

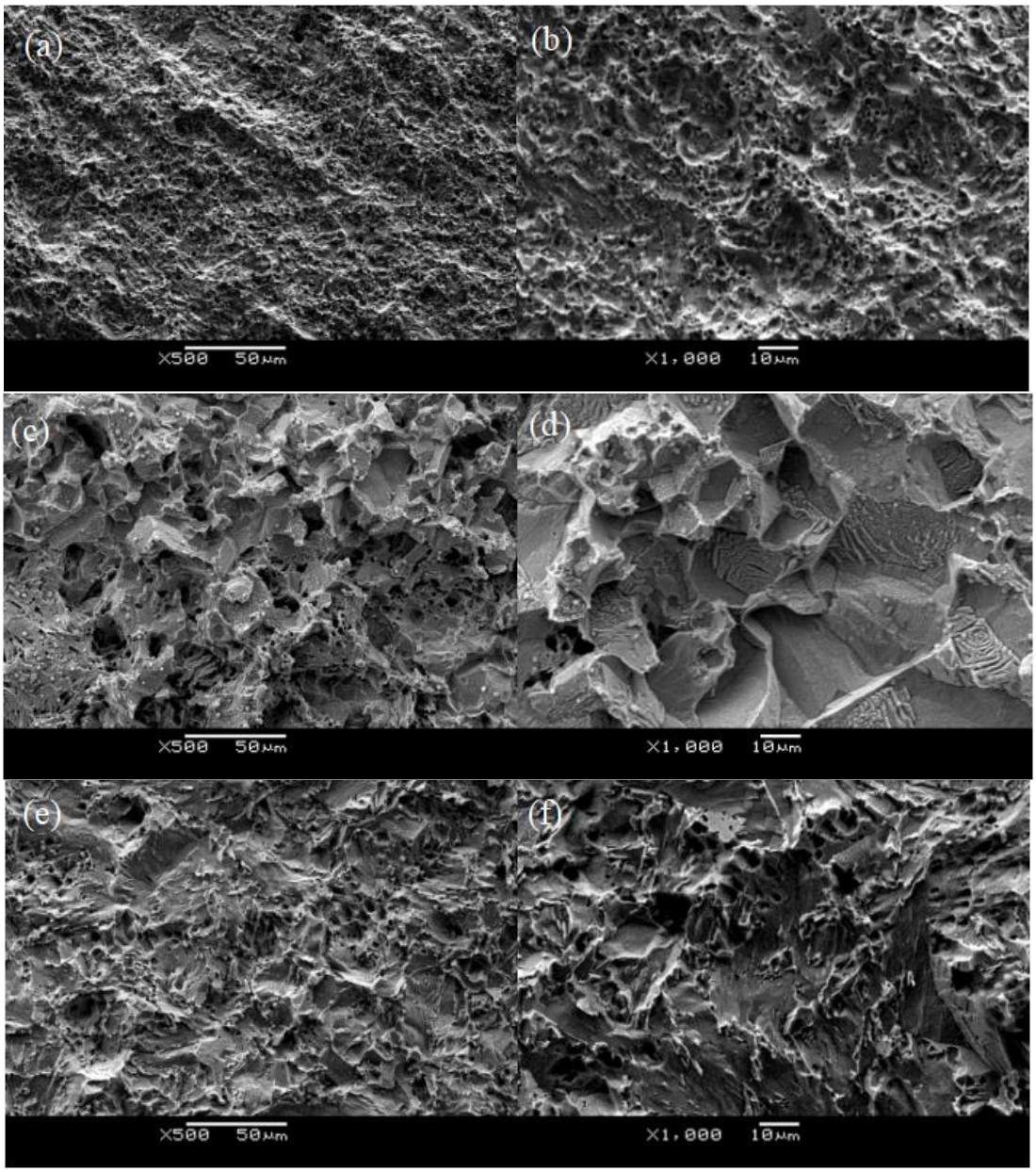

Figure 11. Surface corrosion morphology of X100 steels with different microstructure after removing corrosion products:**(a,b)**hot-rolled;**(c,d)**annealed; **(e,f)**normalized

As shown in Fig.11 (a) and (b), many corrosion pits are observed on the surface of the X100 steel with hot-rolled microstructure, and some small-sized pits gradually integrate together to form large-scale corrosion pits. From Fig. 11(c) and (d), it can be observed that the number of pits is more,

and degree of corrosion is more serious. On the surface of annealed microstructure steel, the pits are deep and large. Fig. 11(e) and (f) reveals the corrosion pits of normalized structure steel is relatively less than that of the above two structures. Therefore, the distribution and characteristics of corrosion pits demonstrate that annealed microstructure is most susceptible to corrosion, the normalized microstructure is the most resistant to corrosion, and the hot rolled structure is between the two, which is consistent with the above corrosion rate results.

To further analyze the AC corrosion behavior of X100 steel with different microstructure, explore the law of pits distribution and the effects of microstructure to the steels with various microstructures, the pitting distribution is shown in Fig.12. Fig.12 (a) exhibits that the pitting of the hot-rolled microstructure mostly appears in the concentrated area of the granular bainite, and partially occurs in the interior of the ferrite grains, where near the grain boundary. As seen in Fig.12 (b), there are some deep pits at the adjacent of ferrite and pearlite, and these etch pits are larger than that of the hot-rolled structure and the normalized structure. Fig.12 (c) shows that the pits on the normalized microstructure are smaller than the above two structures.

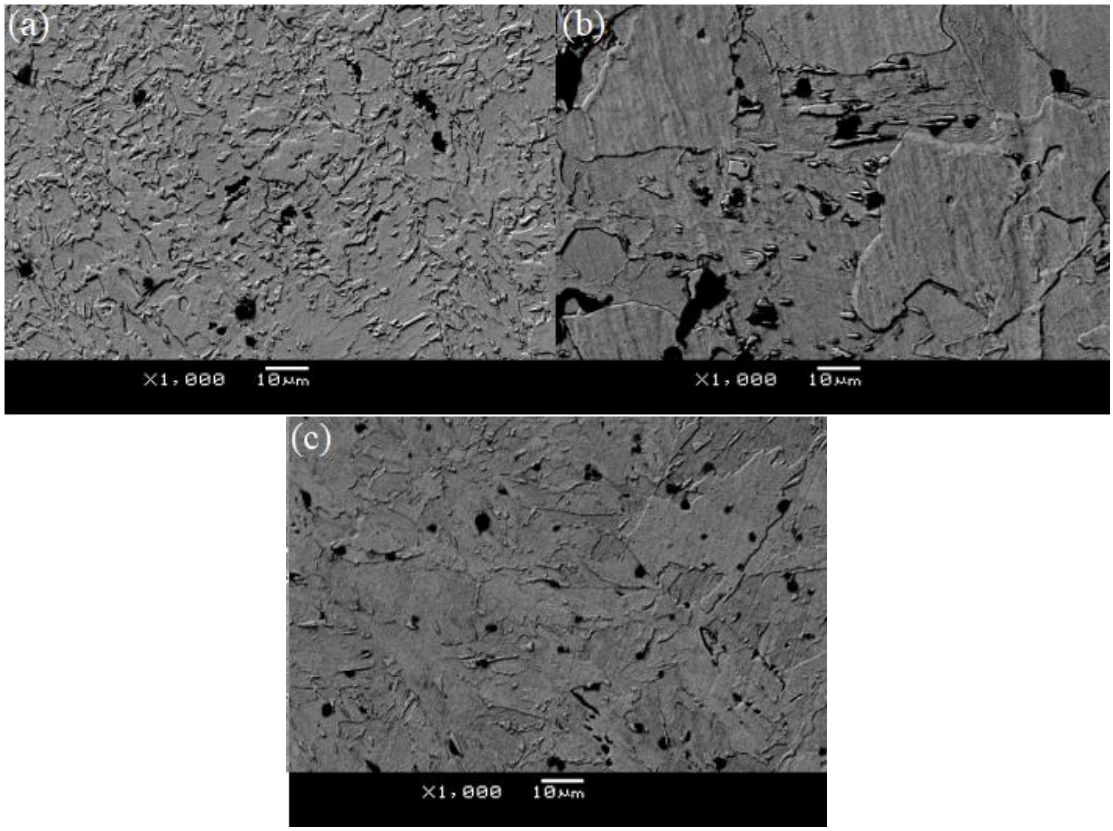

Figure 12. Pitting distribution of X100 steels with different microstructure after removing corrosion products: **(a)**hot-rolled;**(b)**annealed;**(c)**normalized

3.5 Electrochemical test under different temperature with AC application

In order to explore the combined effect of corrosion behavior of temperature and alternating current, choose the hot-rolled microstructure as the electrochemical test sample. The potential sweep

range is -300 (vs SCE) ~ -1000 mV (vs SCE), the scan rate is 1 mV/s and the temperature is controlled at 35℃, 45℃ and 55℃ respectively. Fig.13 reveals the potentiodynamic polarization curves of hot-rolled microstructure steel under different AC current densities at various temperatures. The corrosion current densities obtained by fitting from Fig.13 are shown in Fig.14.

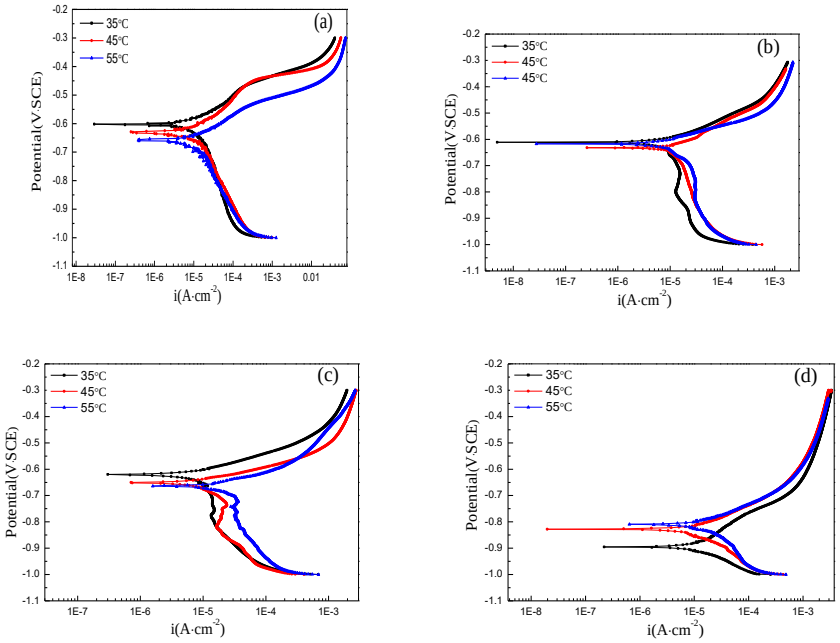

Figure 13. Potentiodynamic polarization curves of hot-rolled microstructure steel under different AC current densities at various temperatures in alkaline soil simulation solution:**(a)**0 A·m^{-2} ; **(b)**30 A·m^{-2};**(c)** 50 A·m^{-2};**(d)** 150 A·m^{-2}

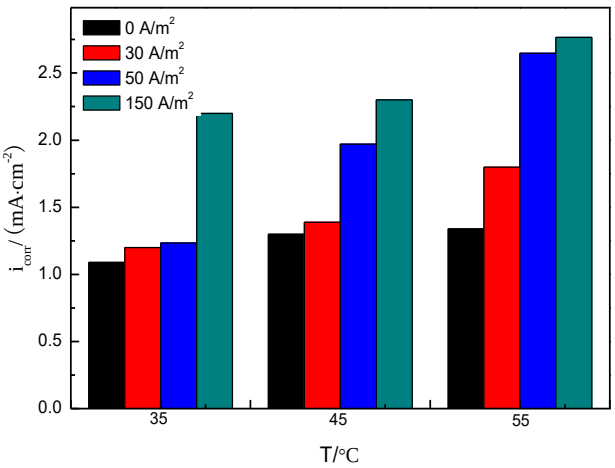

Figure 14. Corrosion current density (i_{corr}) of X100 steel with hot-rolled microstructure under different AC densities at various temperatures in alkaline soil simulation solution

As seen in Fig.13, the characteristics of the cathode and anode curve are similar to the experimental investigation above, which shown in Fig.7. Combined with Fig.13 and Fig.14, it can be seen that at the low temperature (35℃), with the AC current density increases from 0A·m^{-2} to 50 A·m^{-2},

the corrosion current density increases slowly. But the corrosion current density has an enlargement sharply when the applied AC current density increases to 150 $A \cdot m^{-2}$. However, with the increase of temperature to 45℃, there is a sharp increase appearing at the range of AC current density from $30A \cdot m^{-2}$ to 50 $A \cdot m^{-2}$, and this phenomenon is more obvious at 55℃.That indicates that the increase of temperature can promote the corrosion of X100 pipeline steel. At the low AC current density, the effect of temperature on corrosion behavior is more serious. While the AC current density is higher at $150A \cdot m^{-2}$, the AC corrosion plays a dominant role in the X100 steel.

4. DISCUSSION

4.1. The influence of AC current density

Under the high AC current density, the AC potential on the surface of the sample increases instantaneously. Due to the action of the faraday part of the alternating current, it is more conducive to the precipitation of hydrogen and the corrosion of steel is intensified [21]. As the AC current density increases, the internal electric field intensity of the solution increases, which accelerates the diffusion rate of ions (such as H^+) in the solution, and the metal electrode/solution interface is more unstable. On the other hand, under the AC current density, the concentration of dissolved oxygen at the interface may be lower due to the heat effect, and the oxygen absorption reaction is weakened, which is beneficial to the hydrogen evolution reaction of the cathode. So due to the high AC current density, the hydrogen evolution reaction gradually increases and finally dominates the entire cathodic reaction.

4.2. The influence of different microstructure

The corrosion behavior of the X100 steels with different microstructure is various. In the hot-rolled microstructure, GB is composed of carbon-rich austenite and a small amount of M/A, which has high electrochemical activity and is distributed on ferrite. Pitting corrosion is usually easy to occur around this microstructure. At the same time, the micro-galvanic corrosion reaction occurs between GB and AF, which promotes the corrosion rate of the material, so the dispersed of GB leads to the decrease of corrosion resistance of the hot-rolled structure.

Because pearlite is a eutectoid mixture composed with two phases of ferrite and cementite, there presences potential difference between the two phases. Fig.11 (d) clearly shows that there are some small pits inside the pearlite, which indicates some micro-galvanic corrosion appeared inside that. And the quasi-polygonal ferrite as the anode phase and the pearlite as the cathode conform a large number of micro-galvanic corrosion cells, which greatly accelerate the corrosion of the annealed microstructure steel. It can be observed from Fig.11 (d) that pitting corrosion occurs at the junction of ferrite and pearlite and close to the ferrite grain boundary edge, so the corrosion rate of the annealed microstructure of X100 steel is larger. Combined with the corrosion rate (Fig.10), it is known that the annealed structure has the worst corrosion resistance.

Figure 1(e) and (f) reveals the number of small needle-shaped M/A islands in the normalized microstructure increases significantly. In the normalizing process, the transformation is from

supercooled austenite to ferrite through continuous cooling. As the solid solubility of ferrite to carbon is low, the carbon exceeding the solid solubility is excluded into the untransformed austenite, which resulting in the rich carbon accumulation in austenite and further enhancing the stability of austenite [22]. Most of the carbon-rich supercooled austenite will be transformed into martensite during the subsequent cooling process, and a small amount of residual austenite will be retained at room temperature due to incomplete transformation. Then the above two microstructure are mixed to form M/A island [23]. Katiyar et al. [24] demonstrated that the variation in the corrosion rate has been attributed to the shape, size, and distribution of microstructure. So the presence of needle-shaped M/A conduces the normalized microstructure exhibiting better corrosion resistance than the other two. Thus the microstructure of the X100 steel after normalizing has larger corrosion resistance and the lowest corrosion rate.

4. CONCLUSIONS

(1) With the increase of AC current density, the corrosion current density of X100 steel with different microstructure has an increasing trend. And the cathode reaction of the polarization curve is dominated by oxygen consumption reaction without AC interference. But the hydrogen evolution reaction is gradually enhanced as the increase of AC current density. While the AC interference current density is 150 $A \cdot m^{-2}$, the hydrogen evolution reaction dominates the entire cathode process.

(2) The microstructure of corrosion resistance is normalized > hot rolled > annealed. The corrosion of the annealed microstructure is aggravated by the micro-galvanic corrosion formed by pearlite and ferrite. The corrosion resistance of hot-rolled structure is low because of the existence of granular bainite. The normalized structure has more M/A, which exhibits better corrosion resistance.

(3) The increase of temperature will promote AC interference corrosion to a certain extent. At the low AC current density, the increase of temperature influences corrosion behavior markedly. When the AC current density is higher, the AC corrosion plays a dominant role.

ACKNOWLEDGEMENTS
This work was support by the National Natural Science Foundation of China, the Natural Science Foundation of Zhejiang province (No. LY18E010004), and the National R&D Infrastructure and Facility Development Program of China (No. 2005DKA10400).

References

1. R.A. Gummow, R.G.Wakelin and S.M.Segall, AC Corrosion-a New Challenge to Pipeline Integrity, CORROSION 1998, Houston, America, 1998, 566.
2. Y. Hosokawa, F. Kajiyama and T. Fukuoka, *Corrosion*, 60(2004)408.
3. S.B. Lalvani and G. Zhang, *Corros. Sci.*, 37(1995)1583.
4. D. Kuang and Y.F. Cheng, *Corros. Sci.*, 85(2014)304.
5. H.X.Wan, D.D.Song, Z.Y.Liu, C.W.Du, Z.P.Zeng, Z.G.Wang, D.Ding and X.G. Li, *Constr. Build. Mater.*, 154(2017)580.

6. L.Y. Xu, X. Su, Z.X. Yin, Y.H. Tang and Y.F. Cheng, *Corros. Sci.*, 61(2012)215.
7. M.Zhu, C.W.Du, X.G.Li, Z.Y.Liu, H.Li and D.W.Zhang, *Corros. Sci.*, 87(2014)224.
8. M.Zhu, C.W.Du, X.G.Li and Z.Y. Liu, *Corrosion*, 70(2014)1181.
9. M.Zhu, C.W.Du, X.G.Li, Z.Y.Liu, S.R.Wang, J.K. Li and D.W.Zhang, *Electrochim. Acta*, 117(2014) 351.
10. F.F. Eliyan, E.S. Mahdi and A. Alfantazi, *Corros. Sci.*, 58(2012)181.
11. I.M. Gadala and A. Alfantazi, *Corros. Sci.*, 82(2014)45.
12. V. Giorgetti, E.A. Santos, J.B. Marcomini and V.L. Sordi, *Int. J. Pres. Ves. Pip.*, 169(2019)223.
13. B. Jegdić, B. Bobić, B. Radojković, B. Alić and L.Radovanović, *J. Mater. Process. Tech.*, 266(2019)579.
14. Y. Fan, M. Wu, X. Chen and X. Meng, *Corros. Sci. Prot. Technol.*, 28(2016)415.
15. X. Chen, H. Chen and L. Zhang, Corrosion Behavior of X80 Pipeline Steel in Typical Soil Simulation Solutions of West-East Gas Pipeline II, ICPTT 2013, Wuhan, China, 2013.
16. L. Zhang, X.G. Li, C.W. Du and Y. Huang, *Mater. Design.*, 30(2009)2259.
17. S.M. Bhola, F.M. Alabbas, R. Bhola, J.R. Spear, B. Mishraa, D.L. Olson and A.E. Kakpovbia, *Eng. Fail. Anal.*, 36(2014)92.
18. F.M. Alabbas, S.M. Bhola, J.R. Spear, D.L. Olson and B. Mishra, *Eng. Fail. Anal.*, 33(2013)222.
19. K. Al-Muhanna and K. Habib, *Desalination*, 250(2010)404.
20. X. Li, F. Xie, D. Wang, C.H. Xu, M. Wu, D.X. Sun and J.J.Qi, *Eng. Fail. Anal.*, 91(2018)275.
21. H.R. Wang, C.W. Du, Z.Y. Liu, L.T. Wang and D. Ding, *Nanomaterials-Basel*, 10(2017)851.
22. M. Zeng, S.P. Hu, Z.Z. Zhao, H.T. Jiang and Z. Wang, *Mater. Mech. Eng.*, 35(2011)29.
23. X.H. Nie. X.G. Li. C.W. Du and Y.F. Cheng, *J.Appl. Electrochem.*, 39(2009)277.
24. P.K. Katiyar, S. Misra and K. Mondal, *Metall. Mater. Tran.*, 50(2019)1489.